Translational Oncology 14 (2021) 101013

Contents lists available at ScienceDirect

Translational Oncology

journal homepage: www.elsevier.com/locate/tranon

Original Research

Genome-wide analysis of copy number alterations led to the characterisation of PDCD10 as oncogene in ovarian cancer

Carmela De Marco[a,*], Pietro Zoppoli[a], Nicola Rinaldo[b], Sandro Morganella[b], Matteo Morello[c], Valeria Zuccalà[d], Maria Vincenza Carriero[e], Donatella Malanga[a], Roberta Chirillo[a], Paola Bruni[f], Carmine Malzoni[f], Dolores Di Vizio[c], Roberta Venturella[g], Fulvio Zullo[g], Antonia Rizzuto[h], Michele Ceccarelli[b], Gennaro Ciliberto[i], Giuseppe Viglietto[a,*]

[a] Department of Experimental and Clinical Medicine, "Magna Graecia", University Catanzaro, Italy
[b] Biogem Scarl, Institute for Genetic Research "G. Salvatore", Ariano Irpino (AV), Italy
[c] Samuel Oschin Comprehensive Cancer Institute, Cedars-Sinai Medical Center, Los Angeles (CA), USA
[d] Pathology Unit, "Pugliese-Ciaccio" Hospital, Catanzaro, Italy
[e] IRCCS, National Cancer Institute of Naples "Fondazione G. Pascale", Naples, Italy
[f] Casa di Cura "Malzoni-Villa dei Platani", Avellino, Italy
[g] Unit of Obstetrics and Gynaecology, "Magna Graecia" University of Catanzaro, Italy
[h] Department of Medical and Surgical Sciences, "Magna Graecia", Catanzaro, Italy
[i] IRCCS, National Cancer Institute Regina Elena, Rome, Italy

ARTICLE INFO

Keywords:
Copy number alterations
Ovarian cancer
PDCD10

ABSTRACT

Copy Number Alterations (CNAs) represent the most common genetic alterations identified in ovarian cancer cells, being responsible for the extensive genomic instability observed in this cancer. Here we report the identification of CNAs in a cohort of Italian patients affected by ovarian cancer performed by SNP-based array.

Our analysis allowed the identification of 201 significantly altered chromosomal bands (70 copy number gains; 131 copy number losses). The 3300 genes subjected to CNA identified here were compared to those present in the TCGA dataset. The analysis allowed the identification of 11 genes with increased CN and mRNA expression (PDCD10, EBAG9, NUDCD1, ENY2, CSNK2A1, TBC1D20, ZCCHC3, STARD3, C19orf12, POP4, UQCRFS1). PDCD10 was selected for further studies because of the highest frequency of CNA.

PDCD10 was found, by immunostaining of three different Tissue Micro Arrays, to be over-expressed in the majority of ovarian primary cancer samples and in metastatic lesions. Moreover, significant correlations were found in specific subsets of patients, between increased PDCD10 expression and grade ($p < 0.005$), nodal involvement ($p < 0.05$) or advanced FIGO stage ($p < 0.01$).

Finally, manipulation of PDCD10 expression by shRNA in ovarian cancer cells (OVCAR-5 and OVCA429) demonstrated a positive role for PDCD10 in the control of cell growth and motility *in vitro* and tumorigenicity *in vivo*.

In conclusion, this study allowed the identification of novel genes subjected to copy number alterations in ovarian cancer. In particular, the results reported here point to a prominent role of PDCD10 as a *bona fide* oncogene.

Introduction

Cancer is driven by the sequential acquisition of genetic alterations of somatic nature. Genetic alterations identified in cancer cells include single nucleotide variations (SNVs), copy-number alterations (CNAs) and gene fusions.

CNAs represent by far the most common alterations identified in cancer cells, and may cause both gain or loss of DNA fragments. CNAs may contribute to cancer development by inappropriate activation of proto-oncogenes such as EGFR or ERBB2 and/or inactivation of tumor suppressor genes such as pRB or TP53 [1].

Ovarian cancer (OC) is a complex disease that exhibits heterogeneity at both clinical and molecular level. OCs are typically classified as low-

* Corresponding author.
E-mail addresses: cdemarco@unicz.it (C. De Marco), viglietto@unicz.it (G. Viglietto).

https://doi.org/10.1016/j.tranon.2021.101013
Received 14 October 2020; Received in revised form 4 December 2020; Accepted 4 January 2021

or high-grade. Low-grade tumours are driven by activating mutations of RAS and PIK3CA or by loss of PTEN but are typically wild-type for TP53. Conversely, high-grade OCs are mutant for TP53, BRCA1 and/or BRCA2 [2].

CNAs represent relevant components of the genetic variation that affects OC [3]. Accordingly, a large-scale study performed on high-grade OCs performed by The Cancer Genome Atlas Project (TCGA) has suggested that high-grade tumors are more frequently characterized by extensive chromosomal instability than somatic mutations [4].

Here we report on the identification of CNAs in a cohort of primary epithelial OCs by use of a high-resolution SNP Array. Significant alterations were annotated in 3300 altered genes, including the Programmed Cell Death 10 (PDCD10), which was selected for further studies because of its over-expression in the majority of primary and metastatic OCs. PDCD10, also known as CCM3, belongs to the CCM family of proteins and was first identified as one of the genes responsible for Cerebral Cavernous Malformations [5]. Subsequently, it was shown to promote assembly of the Golgi complex, cell proliferation and migration [6,7].

Notably, a significant correlation was found between increased PDCD10 expression and grade, nodal involvement or FIGO stage. In addition, manipulation of PDCD10 expression in OC cells demonstrated that this gene positively regulates cell growth and motility *in vitro* and tumorigenicity *in vivo*. In conclusion, the results reported here point to a prominent role for PDCD10 in OC development.

Materials and methods

Patients

Frozen biopsies of OCs for CN analysis and archive material from 98 patients included in TMA_OC3 and TMA_OC4 were collected from the Unit of Gynecology at the Hospital "Villa dei Platani" (Avellino, Italy) and University Magna Graecia of Catanzaro (Catanzaro, Italy). Ovary2_TMA included samples ($N = 213$) collected from OC patients undergoing surgery at the European Institute of Oncology (Milano, Italy). See Table S1 and S2 for details.

Patient accrual was approved by the Institutional Review Board of the AOU Mater Domini/University Magna Graecia (Catanzaro, Italy). All procedures were performed according to the principles expressed in the Declaration of Helsinki. Written informed consent was obtained from all participants to the study. Patients were surgically staged according to International Federation of Gynaecology and Obstetrics (FIGO) criteria (Cancer Committee of the International Federation of Gynaecology and Obstetrics, 1986). Patient diagnosis was made according to the World Health Organization (WHO) criteria [8].

Representative areas were first selected on haematoxylin–eosin-stained tumour sections by a trained pathologist and a core biopsy for tumour and metastasis blocks were included into the TMA. TMAs were assembled onto a custom-built tissue arrayer (Beecher Instruments, Sun Prairie, WI, USA).

Identification of CN alterations

DNA from OC ($N = 57$) and peripheral lymphocytes ($N = 4$) were hybridized on Illumina (Infinium HD Human610-Quadv) SNP chips (Illumina, San Diego, CA, USA). The log2 ratio of the normalized R values for the probes divided by the expected normalized R values were estimated according to GenomeStudio algorithm. CNV-partition (a GenomeStudio plugin) computed the resulting CN values and confidence for all chromosomal regions in each sample.

Probe position was annotated by using hg18 (NCBI 36) human genome assembly (https://www.ncbi.nlm.nih.gov/assembly/2928). CN alterations were identified using the R/bioconductor package GAIA [9]. CN alterations detected in at least 2 control blood samples were excluded from the analysis.

TCGA data download and analysis

Gene expression data, CNA, GISTIC2 calls and clinical data of patients with serous ovarian cancer S-OC) present in the TCGA database ($N = 406$) were downloaded from UCSC cancer genomics browser (https://genome-cancer.ucsc.edu/; [10]).

CN alterations were defined with an absolute value of CN>0.3. Gene diploid status was set at 0. Thresholds were selected after visual inspection of the density plots relative to the whole dataset, being GISTIC background threshold set at 0.3.

Genes that presented CN alterations that were reflected into altered mRNA expression were identified by linear regression analysis of mRNA levels and CN status in the TCGA dataset. The threshold was arbitrarily set at R^2>0.45.

Immunohistochemistry

Immunostaining was performed using the avidin-biotin-peroxidase method (LSAB kit; DAKO, Glostrup, Denmark) according to manufacturer instructions. Anti-PDCD10 was from Sigma-Aldrich (St. Louis, MO, USA) (#HPA027095).

The immunohistochemical score for the PDCD10 antibody used in this work was selected on the basis of methods widely accepted and used in previous studies [11,12]. Every tumor was given a score according to the intensity of the cytoplasmic staining (no staining = 0, weak staining = 1, moderate staining = 2, strong staining = 3) and the extent of stained cells (0% = 0, 1–10% = 1, 11–50% = 2, 51–80% = 3, 81–100% = 4). The final immunoreactive score was determined by multiplying the intensity scores with the extent of positivity scores of stained cells, with the minimum score of 0 and a maximum score of 12. For the interpretation of the results, immunostaining was defined negative for scores from 0 to 4, and positive for scores from 6 to 12. Sections were evaluated blindly by two expert pathologists (DDV, VZ).

RT-PCR and Q-PCR

Total RNA and DNA were prepared by standard methods. cDNA was synthesized from 1μg of total RNA using cDNA Reverse Trascription Kit (ThermoFisher, Waltam, MA, USA). RT-PCR and Q-PCR were performed using the Power SYBR Green PCR Master Mix with the QuantStudio 12K Flex Real Time System (ThermoFisher), as previously described [13]. Normalization was performed to GAPDH mRNA/DNA content. The relative amounts of mRNA or DNA were calculated by the comparative cycle threshold (CT) method.

Cell lines

OVCAR-5 and OVCA429 cells were kindly provided by Dr. Gustavo Baldassarre (C.R.O, Aviano, Italy) and cultured in RPMI 1640 (Lonza, Walkersville, MD, USA) supplemented with 10% FBS (Sigma-Aldrich) and 100 units/ml penicillin-streptomycin (Lonza). Cells were authenticated by STR profile at DSMZ (Braunschweig, DE) and used within 6 months.

Virus generation and infection

Lentiviral particles were generated in HEK293T packaging cells using the Human PDCD10 (NM_006218) MISSION shRNA set and the Mission non-target control transduction virus (SHC002V) (Sigma-Aldrich) as described before [14]. After transfection, supernatants were collected at 8 hour intervals, filtered and used for three rounds of transduction by spin infection with 8μg/ml polybrene (Sigma-Aldrich). Transduced cells were selected with 0.5μg/ml puromycin (Invitrogen).

Western Blot and Rho-GTP pull-down assays

Whole cell extracts were prepared and transferred to membranes with standard methods as described before [15]. Membranes were incubated overnight at 4°C with the following antibodies: anti-PDCD10 (#SAB1305161), anti-β-Actin (clone AC-74, #A2228) from Sigma-Aldrich; anti-phospho cofilin (sc-12912), anti-cofilin (sc-33779) and anti- Cyclin D1 (sc-8396) from Santa Cruz (Dallas, TX, USA); anti-phospho-Mypt1 (#5163), anti-Mypt1 (#2634), anti-phospho-MLC2 (#3671), anti-MLC2 (#8505) and anti-PARP (#9542) from Cell Signaling Technology (Danvers, MA, USA); anti-cleaved Caspase 3 (2305-PC-100) from Trevigen (Gaithersburg, MD, USA). GTP-bound Rho was assayed with Rho assay reagent according to manifacturer instructions (#17-294; Millipore, Burlington, MA, USA). Chemio-luminescence was detected with Alliance Mini WL2M system (Uvitec, Cambridge, UK).

Cell viability assay and propidium iodide (PI) staining

Cells were plated at a density of 1×10^3/well in triplicate and daily counted by MTT assay. Before harvesting, the cells were left with MTT reagent (5 μg/mL, Sigma-Aldrich) at 37 °C for 4 h. Formed formazan as an indicator of cell viability was solubilized by adding 100 μL DMSO into each well. The extent of formazan production was determined by a microplate reader (Multiskan FC, Thermo Fisher Scientific) at 570 nm, while 690 nm served as the reference wavelength. The experiment was repeated at least three times.

Cell cycle distribution was analysed by flow cytometry. In brief, 10^6 cells were harvested in phosphate-buffered saline (PBS) and fixed O.N. at -20 °C in ethanol (70%). Fixed cells were washed once in PBS and stained with 50 μg/ml of propidium iodide, 0.01% NP40 and 0.1 mg/ml RNase A in PBS for 30 min (Thermo Fisher). Stained cells were analysed with a fluorescence-activated cell sorter (FACS) LSRFortessa X20 (Becton-Dickinson, Franklin Lakes, NJ), and data were generated with the FloJo cell software (Becton-Dickinson).

Caspase activity assay

Caspase 3/7 activity was measured with Caspase-Glo assay kit (Promega, Madison USA) according to the manufacturer instructions. Briefly, the plates containing not synchronized cells were removed from the incubator and allowed to equilibrate to room temperature for 30 min. 100 μl of Caspase-Glo reagent was added to each well and gently mixed with a plate shaker at 300–500 rpm for 30 s. Plates were then incubated at RT for 2 h. The luminescence of each sample was measured in a plate-reading luminometer (Luminoskan Ascent, Thermo Scientific). The experiments were performed in triplicate.

Soft agar assay

Cells (2.5×10^3) were suspended in RPMI medium containing 0.35% low-melting agarose (Type VII, Sigma-Aldrich) and seeded onto 0.5% low-melting agarose in six-well tissue culture plates. Colonies were scored after 3 weeks in 5 randomly selected fields/well, at 4X magnification. Photographs were also taken at higher magnification (40X) to measure clone size. Clones were classified according to their diameter in > 200 μm or <200 μm.

Tumor formation assays

Cells harvested from culture plates were resuspended in 200 μl of 1:1 Matrigel in PBS and injected subcutaneously into 6 week-old athymic CD1 mice (Charles River Laboratories International, Inc., Wilmington, MA, USA). Tumour size was calculated weekly as length × width × width/2 with a caliper.

Migration assay

Cells (5×10^4) were seeded in the upper chamber of Transwell polycarbonate filters (Sigma-Aldrich) with 8-μm pore size and incubated for 48 h at 37 °C in serum-free medium. Cells that did not migrate through the pores were manually removed with a cotton swab. Cells migrated to the bottom of the membrane were fixed in cold methanol for 10 min, stained with 0.01% crystal violet in 20% ethanol and counted in 5 fields/well in triplicate experiments.

Analysis of cytoskeleton

To analyse cytoskeletal organization, cells grown on glass slides to semi-confluence were fixed with 2.5% formaldehyde, permeabilized with 0.1% Triton X-100 for 10 min at 4 °C, and then incubated with 0.1 μg/ml rhodamine-conjugated phalloidin (Sigma-Aldrich) for 40 min. After nuclear staining with 4-6-diamidino-2-phenylindole dye (DAPI), cells were analyzed by a fluorescence inverted microscope connected to a camera (Carl Zeiss, Oberkochen, DE).

Statistical analysis

Association between PDCD10 expression and clinic-pathologic variables was evaluated by using Fisher's exact test. Continuous variables were analyzed by two tailed Student's t test or Two-way ANOVA as indicated in the text (GraphPad Software, Inc., La Jolla, CA, USA). Statistical significance was set at $p < 0.05$.

Results

Identification of chromosomal regions subjected to CNA in OC

We have processed 57 OC samples for CNA analysis using the Illumina BeadStudio SNP based 610K Array. Analysed samples included 35 serous ovarian carcinomas (S-OCs), 7 endometrioid ovarian carcinomas (E-OCs), 5 mucinous ovarian carcinomas (Mu-OCs), 3 clear cell ovarian carcinomas (CC-OCs) and 7 mixed-type ovarian carcinomas (MX-OCs). As control, we made use of peripheral blood samples from 4 patients.

The values of log2 ratio of signal intensity were estimated according to the GenomeStudio algorithm. CNAs detected in the DNA extracted from cancer samples were filtered with those detected in the DNA from pooled control blood samples.

We observed that most OCs presented distinct increases and/or decreases of the log2 ratio of signal intensity that spanned large portions of most chromosomes. Identified CNAs were classified according to Mermel and coworkers [16] as homozygous deletions, heterozygous deletions, low-level CN gains and high-level CN gains.

To identify regions that were most frequently subjected to CNAs, we used Genomic Analysis of Important Aberrations (GAIA.), a statistical method that allows identification of regions containing CNAs with a threshold of q-value < 0.25 [9]. By this analysis we identified 201 significant chromosomal bands. Low-level CN gains were observed in 63 chromosome bands, high-level CN gains were observed in 7 chromosome bands, heterozygous deletions were observed in 93 chromosome bands and homozygous deletions were observed in 38 chromosome bands. See Supplementary File S1 for a comprehensive list of identified CNAs.

S-OC represents by far the most abundant subtype of OC. Bands 1q43-44, 3p12.1, 3q26.1, 8q23-24, 11q14.1, 11q21-22, 13q33 were frequently subjected to CN gain (>50% of samples) whereas bands 17p11.2, 19p13.3 and 11p15.5 were frequently subjected to CN loss (frequency >30%) (Fig. 1A). The complete list of bands subjected to CNAs in S-OC is reported in Supplementary File S1.

GAIA analysis performed on E-OCs ($n = 7$) identified significant (q-value < 0.25) low-level CN gains at bands 1q25.2 and Xq21.1 and homozygous deletions at chromosomal bands 6p21.32 and 11q11 that were specific of E-OC patients. CNA specific of MX-OC patients were

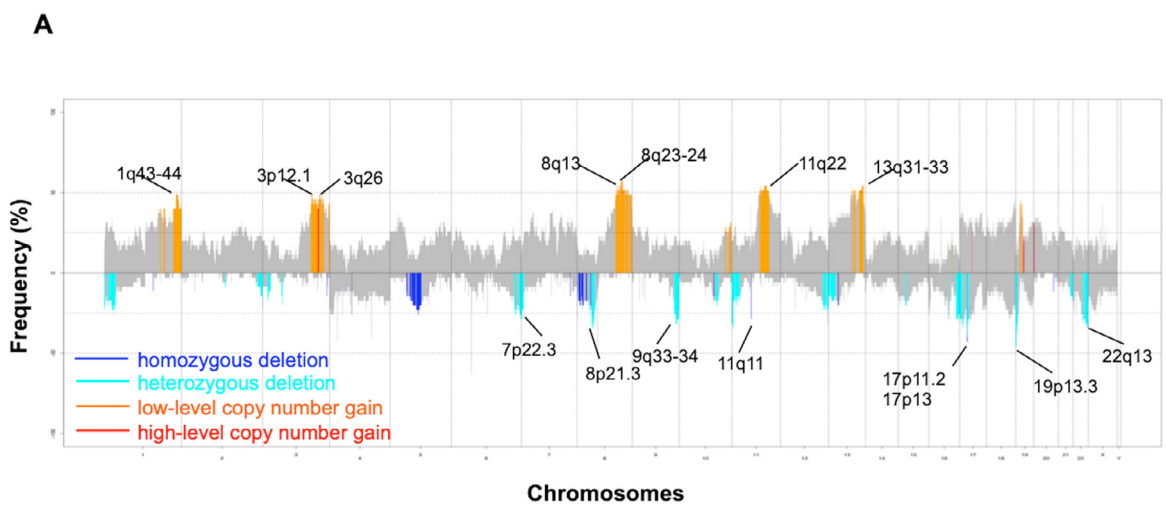

Fig. 1. CNAs and PDCD10 protein expression in S-OCs. A. Overview of genomic alterations identified in S-OC patients. X-axis: chromosome positions; y-axis: frequency (%). Significant alterations are depicted as follows: homozygous deletions (blue), heterozygous deletions (cyan), low-level CN gain (orange) and high-level CN gain (red). Non-significant alterations are reported in grey. Chromosomal bands subjected to CN gains and losses in >50% and >30% of patients are indicated, respectively.

observed at 3q22.1, 7p21.3, 18p11.2 and 18p11.3. Finally, CNA at 16p13.3, 17q21.31 and Xq22.3 were specific of Mu-OC patients (Supplementary File S1).

Identification of genes subjected to CNA in S-OC and comparison with TCGA dataset

The analysis performed here yielded a total of 3300 genes subjected to CNA in S-OC: 576 were CN gains (530 low-level CN gain, 46 high-level CN gain) whereas 2724 genes were subjected to CN loss (2454 heterozygous deletion, 270 homozygous deletion). Chromosomal locations, frequencies of alteration, genomic intervals and names of the genes altered in S-OC are listed in Supplementary File S2.

The results presented here are in agreement with those shown in previous genome-wide studies. Several genes identified here as amplified are located at 3q26.2 (MDS1, MYNN, GPR160, PHC3, PRKCI, SKIL, CLDN11 and TERC) or at 8q24.21 (MYC and PVT1). Similarly, genes identified in this study as subjected to CN losses (DOCK5, CSMDD1, TNFRSF10A/B/C, EGR3, STK11, APC2) have already been identified in previous studies [3,17,18].

Subsequently, we compared the genes subjected to CNA identified in this study with those identified by previously published work and that are annotated in the TCGA dataset, using the GISTIC 2.0 algorithm [16]. This comparison showed that 167 altered chromosomal bands (83%) and 1397 altered genes (42%) identified in this study are annotated in the TCGA dataset (Supplementary File S3). It is of note that among the genes in common between our study and the TCGA, 305 genes presented coherent alteration of their mRNA expression (Supplementary File S4). High-level CN gains with coherent mRNA increase were identified in 11 genes: PDCD10, EBAG9, NUDCD1, ENY2, CSNK2A1, TBC1D20, ZCCHC3, STARD3, C19orf12, POP4, UQCRFS1.

Among these PDCD10 was selected for further studies because of the highest frequency of alteration. This gene, which maps at 3q26, a region already known to be involved in OC, was found to be subjected to high-level CN gain in >47% of S-OC patients. See Table 1.

Increased PDCD10 CN is associated with elevated protein levels in OC

PDCD10 expression was investigated in Tissue Micro Arrays containing duplicated core biopsies of 98 OCs (TMA_OC3 and TMA_OC4, respectively) and 26 normal tissues (16 tubal and 10 endometrium tissues, respectively). Tumors for which PDCD10 staining was available were 93. The evaluation criteria for the staining of the protein are reported in Materials and Methods. Patients' clinical-pathological characteristics are summarized in Supplementary Table S1.

Table 1
Genes that showed simultaneous high-level CN gains in this study and alteration of CN and of mRNA expression in the TCGA dataset.

Gene Symbol	Chromosome band	Frequency of CN gain (%)
PDCD10	3q26.1	47.54
EBAG9	8q23.2	42.62
NUDCD1	8q23.1	42.62
ENY2	8q23.1	42.62
CSNK2A1	20p13	26.23
TBC1D20	20p13	26.23
ZCCHC3	20p13	26.23
STARD3	17q12	22.95
C19orf12	19q12	19.67
POP4	19q12	19.67
UQCRFS1	19q12	19.67

Immunostaining analysis revealed that most of the normal ovary samples (23 out of 26) were negative for PDCD10. On the other hand, 56 out of 93 OCs showed strong cytoplasmic staining for PDCD10 protein (60%; $p < 0.0001$) (Fig. 2A). Increased PDCD10 staining was observed in 60% S-OCs ($n = 39$), 67% E-OCs ($n = 8$), all CC-OCs ($n = 7$) but not in Mu-OCs ($n = 6$). Notably, among the 3 MX-OCs analyzed (1 S-OC/CC-OC, 1 E-OC/CC-OC, 1 S-OC/E-OC), only the 2 tumors with CC component were positive for PDCD10 expression. See Supplementary Table S2 and Fig. 2B-F for representative images.

We also investigated whether the increased expression of PDCD10 protein observed in the TMA studies occurred through mechanisms involving deregulation of its mRNA transcription. To this aim we performed quantitative RT-PCR analysis. As shown in Fig. 2G, we found high PDCD10 mRNA level in 28 out of 38 OCs (68%). Among these, 25 OCs were selected because both mRNA and immunohistochemistry analysis were available (Supplementary Figure S1A). A good correspondence between mRNA levels and protein staining in tissue biopsies was observed: 16/22 samples with strong staining of PDCD10 protein had high mRNA levels and 2/3 samples with negative staining had low PDCD10 mRNA levels (Supplementary Figure S1B). Notably, among the 28 OCs that presented high mRNA levels 8 presented increased gene CN (Supplementary Figure S1C), suggesting that one major mechanism of PDCD10 overexpression in OC is represented by gene amplification.

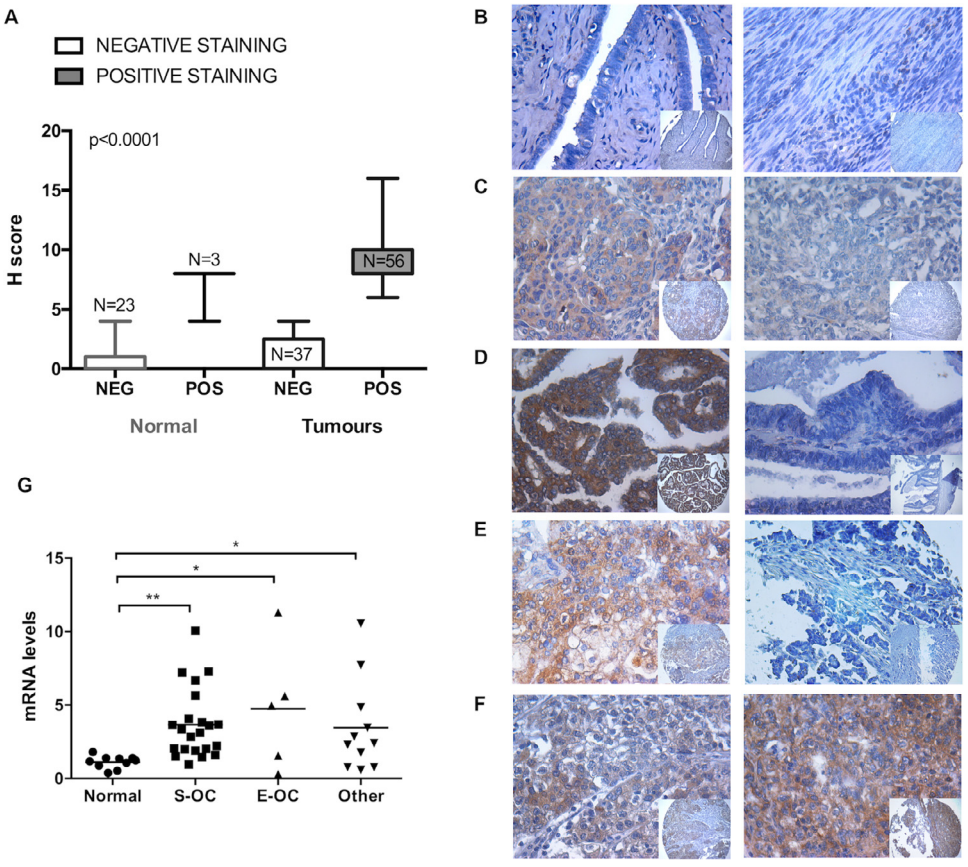

Fig. 2. PDCD10 protein expression in OCs A. The graph summarizes the results of immunostaining for PDCD10 in OCs (N=93) and normal tissues (N=26). ****p<0.0001 (Fisher's exact test). **B-F.** Representative PDCD10 staining of normal or cancerous tissues: **B**, Falloppian tubes (left panel), endometrium (right panel); **C**, S-OCs; **D**, E-OCs; **E**, CC-OC (left panel), Mu-OC (right panel); **F**, Mx-OCs. **G.** Q-RT-PCR analysis of PDCD10 mRNA level in normal and cancer samples. **p<0.005, *p<0.05 (Student's t-test).

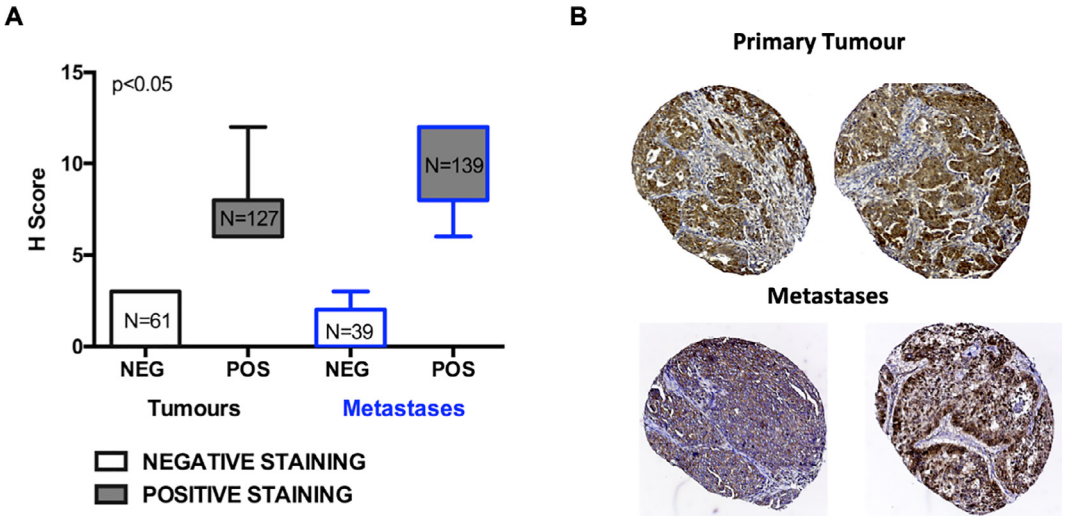

Fig. 3. Protein expression of PDCD10 in matched primary tumors and metastases. A. The graph summarizes the number of samples expressing PDCD10 protein in primary OCs and in the corresponding metastatic lesions. *p<0.05 (Fisher's exact test). **B.** Representative PDCD10 immunostaining of primary tumors (upper panels) and their corresponding metastasis (bottom panels).

PDCD10 protein levels increase in metastatic lesions

Subsequently, we validated PDCD10 expression in an independent TMA (Ovary2_TMA) with matched primary and metastatic OC samples arrayed. Patients' characteristics are summarized in Table S3. This TMA contained core biopsies of 213 OCs and their corresponding metastasis. PDCD10 was expressed in 67% (127 out of 188) of primary tumors analyzed and in 78% (139 out of 178) of the corresponding metastasis (Fig. 3A and Table S4). Representative images are shown in Fig. 3B. We found that a slightly higher number of metastatic lesions expressed PDCD10 compared with primary tumors (78% versus 67%, respectively). See Table S5 and S6 for a detailed patient-by-patient report of PDCD10 staining score.

Then, we correlated PDCD10 expression with clinical-pathologic features. We observed a significant association between the levels of PDCD10 protein and higher tumour grade (G3-G4 vs G1-G2, $p < 0.005$). In addition, a significant fraction of S-OC patients with high PDCD10 expression (27 out of 33, 82%, $p < 0.04$) was positive for nodal involve-

Table 2
Association of PDCD10 with clinical-pathologic features in OC

	OC				S-OC				E-OC			
		PDCD10				PDCD10				PDCD10		
	N	NEG (%)	POS (%)	*P*	N	NEG (%)	POS (%)	*P*	N	NEG (%)	POS (%)	*P*
Age												
<62	85	27 (32)	58 (68)	0.5	70	23 (33)	47 (67)	0.5	15	4 (27)	11 (73)	0.13
≥62	103	34 (33)	69 (67)		79	25 (32)	54 (68)		24	9 (38)	15 (62)	
Grade												
G1-G2	53	25 (47)	28 (53)	**0.01**	47	23 (49)	24 (51)	**0.005**	6	2 (33)	4 (67)	1.00
G3-G4	133	36 (27)	97 (73)		101	25 (25)	76 (75)		32	11 (34)	21 (66)	
FIGO												
I-II-IIIA,B	50	19 (38)	31 (62)	0.21	33	9 (27)	24 (73)	0.5	17	10 (59)	7 (41)	**0.005**
IIIC	138	42 (30)	96 (70)		116	39 (34)	77 (66)		22	3 (14)	19 (86)	
N.I.[a]												
NEG	35	14 (40)	21 (60)	0.09	25	11 (44)	14 (56)	**0.04**	10	3 (30)	7 (70)	1.0
POS	45	10 (22)	35 (78)		33	6 (18)	27 (82)		12	4 (33)	8 (67)	
Tum.Dim[b]												
< 1cm	110	37 (34)	73 (66)	0.7	93	31 (33)	62 (67)	0.7	17	6 (35)	11 (65)	1.0
> 1cm	69	21 (36)	48 (64)		48	14 (29)	34 (71)		21	7 (33)	14 (67)	

[a] Nodal Involvment
[b] Tumor Dimension

ment. Similarly, while no significant correlation was observed between PDCD10 and FIGO stage in non-stratified OCs ($n = 188$), a strong association of PDCD10 expression with FIGO stage was found in E-OC patients ($n = 39$; $p < 0.05$). In particular, 19 out of 22 patients (86%) with high FIGO stage (stage 3C) presented high PDCD10 expression whereas only 7 out of 17 patients (41%) with low FIGO stage (stages 1-3B) presented high PDCD10 expression. See Table 2 for a summary of the results. All together these results suggest that PDCD10 may contribute to OC onset and/or progression.

PDCD10 regulates growth of OC cells both in vitro *and* in vivo

To determine the role of PDCD10 in the transformation of epithelial OC cells we used the cell lines OVCAR-5 and OVCA429, which express high levels of PDCD10 (Supplementary Figure S2). These cellular systems have been well characterized as models of high-grade S-OC [19,20]. OVCAR-5 and OVCA429 cells were mock-transduced (SCR) or transduced with lentivirus carrying different shRNAs to PDCD10 (shPDCD10 #1 and shPDCD10 #2, respectively). OVCAR-5 and OVCA429 cells from different transduction experiments were expanded for further studies.

Analysis of proliferation by Trypan-exclusion assay demonstrated that OVCAR-5 and OVCA429 cells and the corresponding cells silenced for PDCD10 duplicated at a reduced rate in monolayer compared with SCR cells (approximately 1.5- and 2.3-fold decrease, respectively) (Fig. 4A-B). Accordingly, suppression of PDCD10 was associated with decreased phosphorylation of ERK1/2 and pRB and reduced Cyclin D1 protein levels in both cell lines (Fig. 4C).

Flow cytometry analysis (Fig. 4D-G) demonstrated a significant increase in the percentage of cells in G0/G1 phase following PDCD10 knockdown compared with control cells (13.5% for OVCAR-5 cells and 24% for OVCA429 cells on average) with a concomitant decrease in the percentage of cells in the S and G2/M phases ($p < 0.05$). Conversely, PDCD10 silencing induced no change in apoptosis (Supplementary Figure 3). These results indicate that PDCD10 regulates anchorage-dependent proliferation of human epithelial OC cells in culture but not apoptosis.

PDCD10 also regulates anchorage-independent growth *in vitro* and tumorigenicity *in vivo*. In semisolid medium, OVCAR-5-SCR and OVCA429-SCR cells give rise to several large colonies. Conversely, interference for PDCD10 induced a significant decrease in the number of colonies both in OVCAR-5 cells (OVCAR-5-SCR, 42.9 ± 1.5; OVCAR-5-shPDCD10#1 27.8 ± 2.1; OVCAR-5-shPDCD10#2 26.9 ± 0.7, $p < 0.001$) and OVCA429 cells (OVCA429-SCR, 33.4 ± 3.7; OVCA429-shPDCD10#1 22 ± 2; OVCA429-shPDCD10#2 16.4 ± 3.4, $p < 0.05$) (Fig. 4H). In addition, when injected subcutaneously into athymic CD1 mice (3×10^6 cells per mouse), PDCD10-silenced cells promoted tumour formation with longer latency and slower kinetic in comparison with control cells (Fig. 4I). Collectively these data suggest a role for PDCD10 in ovarian tumorigenesis.

PDCD10 regulates migration of ovarian cancer cells

Finally, we investigated the effects of PDCD10 on the capability of OC cells to migrate. To this aim we performed Boyden chamber assays using OVCAR-5 and OVCA429 cells and the corresponding cells silenced for PDCD10. We found that PDCD10 down-regulation induced a significant decrease of migrating cells in comparison to SCR cells in OVCAR-5 and OVCA429 cells (5- and 2-fold on average, respectively, $p < 0.005$). In fact, OVCAR-5-SCR cells presented 66.3 ± 11.3 migrated cells/field; OVCAR-5-shPDCD10#1 cells presented 17.3 ± 3.7 migrated cells; OVCAR-5-shPDCD10#2 cells presented 9.4 ± 3.2 migrated cells (Fig. 5A). OVCA429 cells presented 46.9 ± 11.3 migrated cells/field; OVCA429 shPDCD10#1 cells presented 24 ± 6.5 migrated cells; OVCA429 shPDCD10#2 cells presented 17.5 ± 5.9 migrated cells (Fig. 5B).

These observed changes in cell migration likely reflected the organization of the F-actin cytoskeleton. In agreement with their decreased motility, OVCAR-5 and OVCA429 shPDCD10 cells assumed a larger, flattened morphology and the loss of polarity with random orientation of actin filaments. Conversely, OVCAR-5 and OVCA429 SCR cells exhibit an elongated morphology and display F-actin-rich structures resembling lamellipodia (Fig. 5C).

Cell motility is regulated by the small GTPase RhoA [21]. Therefore, we determined the role exerted by suppression of PDCD10 expression into the RhoA pathway. We found that OVCAR-5 and OVCA-429 shPDCD10 presented a significant increased amount of active Rho (Rho-GTP) as well as increased phosphorylated Cofilin that prevents actin depolymerization. On the contrary, OVCAR-5 and OVCA429 shPDCD10 cells presented reduced phosphorylation of MYPT1 and increased phosphorylation of MLC proteins, both of which are involved in the contraction of acto-myosin (Fig. 5D). These results indicate that PDCD10 positively regulates the migratory potential of human OC cells by impinging on the RhoA pathway.

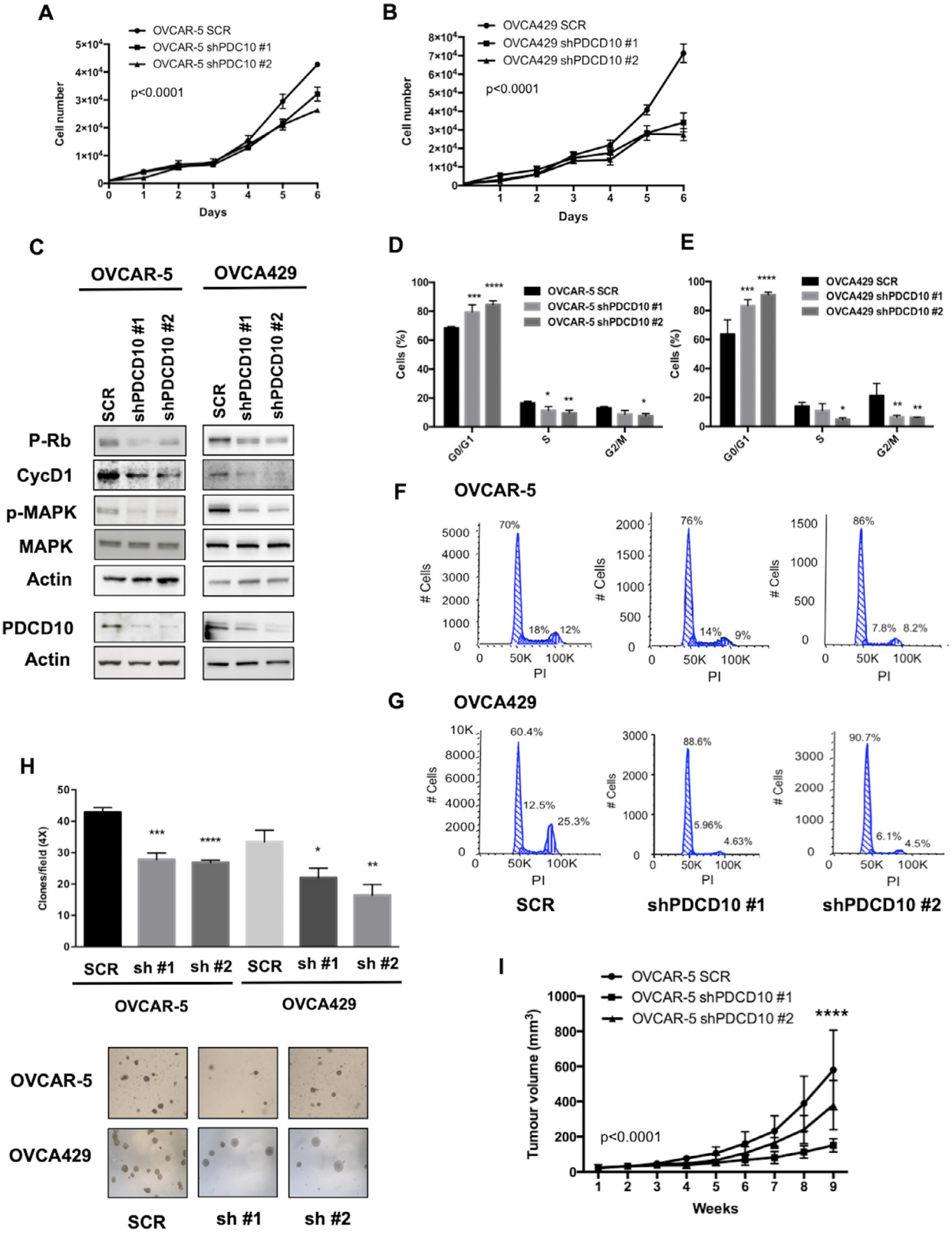

Fig. 4. PDCD10 promotes OC cells growth. A-B. Proliferation rate of OVCAR-5 (**A**) and OVCA429 (**B**) cells and/or clones interfered for PDCD10 expression (shPDCD10 #1 and #2) determined by MTT assay. Data are means (±SD) of triplicate experiments, ****p<0.0001 (Two-Way Anova test). **C.** Immunoblot analysis of indicated proteins: phosphorylated pRB, Cyclin D1, phosphorylated p42/44, total p42/44, actin. PDCD10 is shown as control of the knockdown. Actin was used as loading control. **D-E.** The graphs plot the percentage of OVCAR-5 (**D**) and OVCA429 (**E**) cells and the corresponding cells interfered for PDCD10 (shPDCD10 #1 and #2) in the cell cycle phases. Results are representative of three independent experiments. **** p<0.0005, *** p<0.0005, **p<0.005, *p<0.05 (Student's t-test). **F-G.** Representative plots of Propidium staining and flow cytometry analysis of cell cycle in OVCAR-5 (**F**) and OVCA429 (**G**) cells and the corresponding cells interfered for PDCD10 expression (shPDCD10 #1 and #2). **H.** The graphs report the mean number (±SD) of clones/field generated in anchorage-independent conditions. Representative images of plates are reported at the bottom of the graph (Magnification 20X). **** p<0.0001, *** p<0.0005, **p<0.005, *p<0.05 (Student's t-test). **I.** Tumor growth of OVCAR-5 SCR, OVCAR-5 shPDCD10 #1 and OVCAR-5 shPDCD10 #2, injected in CD1 nude mice (N=8/group). Data are shown as mean ± SD; ****p<0.0001 (Two-Way Anova test).

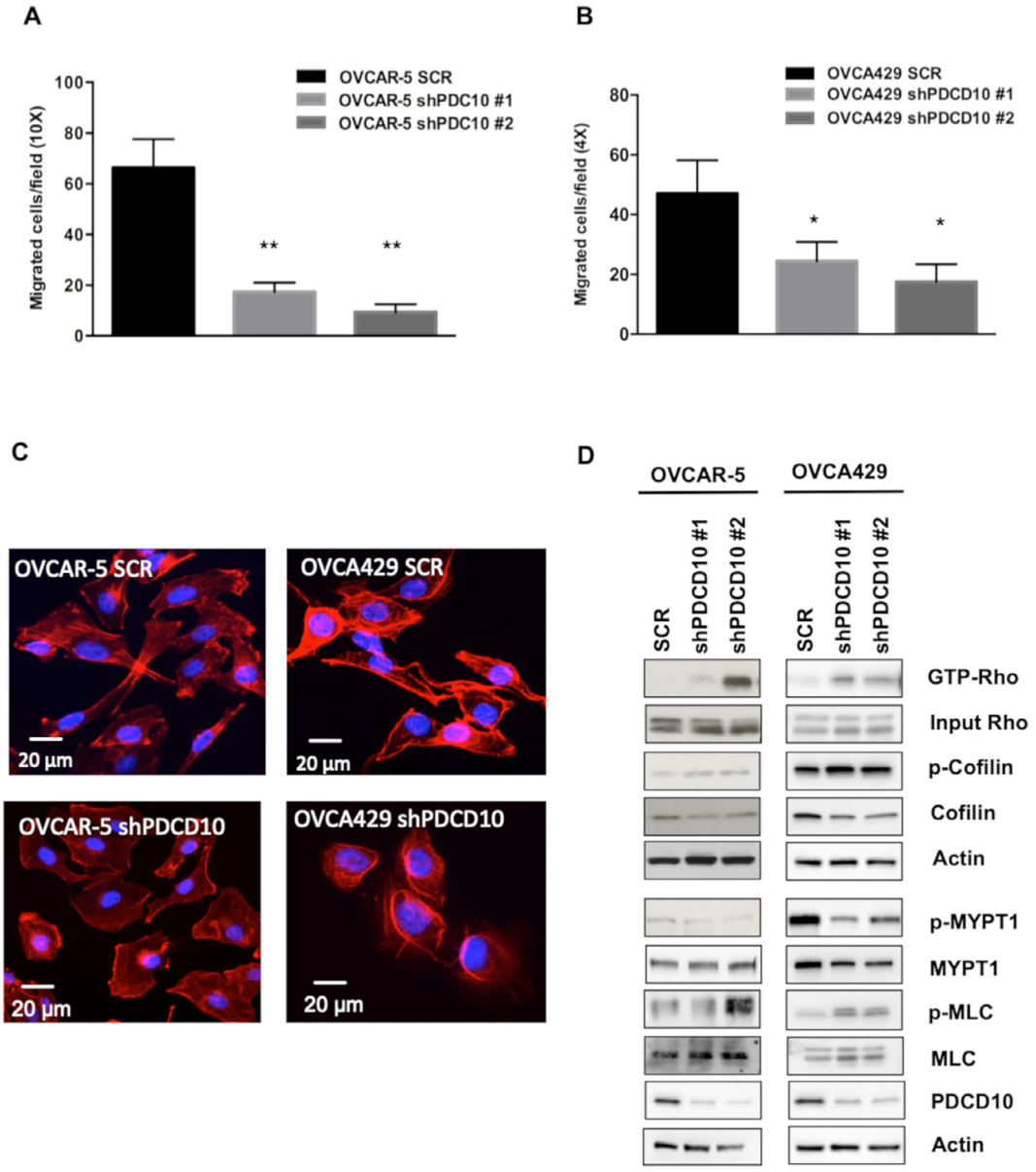

Fig. 5. PDCD10 promotes migration of OVCAR-5 and OVCA429 cells. A. The graph reports the mean number/field (±SD) of OVCAR-5 cells migrated to the bottom of Transwells after 48h. **p<0.005 (Student's t-test). **B.** The graph reports the mean number/field (±SD) of OVCA429 cells migrated to the bottom of Transwells after 48h. *p<0.05 (Student's t-test). **C.** Cytoskeletal organization of OVCAR-5 and OVCA429 silenced for PDCD10. F-actin fibers were stained with rhodamine-phalloidin (red) and nuclei were stained with DAPI (blue). Scale bar: 20 µm. Original magnification: 400X. **D.** Immunoblot analysis of activated RhoA (GTP-Rho) and its downstream substrates (p-Cofilin, Cofilin, p-MYPT1, MYPT1, p-MLC and MLC) in OVCAR-5 and OVCA429 cells. PDCD10 is shown as control of the knockdown. Actin was used as loading control.

Discussion

The first relevant result of this work consists in the identification of 201 chromosomal regions subjected to CNA, most of which contain known oncogenes or tumor suppressor genes in OC [3,17,18]. The novelty of the data described in this manuscript consists in the identification of CN gains and losses in further chromosomal bands that had not been previously associated with OC. In particular, CN gains at 10q26.2 and 13q31 occur specifically in S-OCs, CN gains at 18p11.3 are apparently specific of MX-OCs and CN gains at Xq21.1 are specific of E-OCs. The 10q26.2 band has been described as a susceptibility locus for several tumour types [22,23] whereas the 13q31 region contains a microRNA cluster implicated in tumour growth and chemoresistance [24,25], which also dictates poor prognosis in patients with colorectal cancer [26].

As regards the CN losses, region 9q34 contains the gene responsible for the Tuberous Sclerosis Complex, TSC1 [27], a gene downregulated in breast cancer (LAMC3) [28] and a gene deleted in B-cell lymphoblastic leukemia and bladder cancer (ABL1) [29,30]. Band 22q13 includes a putative tumour suppressor gene (PHF21B) that has been associated with familiar OC [31] and reported to be deleted in head and neck squamous cell carcinoma. Finally, the 17p13.2 band contains the putative tumour suppressor gene KCTD11, which has been implicated in hereditary colorectal cancer [32] and sporadic breast and ovarian cancer [33].

An additional relevant point of this manuscript is the identification, among the genes subjected to CN gains, of PDCD10 as an important player in the onset and/or progression of OC. PDCD10 is located at 3q26.1, a region shown to be amplified in various types of human cancer including OC.

Our data indicate that approximately half of OC patients analysed presents CN gains in the gene encoding PDCD10, which results in a marked increase of mRNA and protein levels. PDCD10 protein is significantly overexpressed in primary and metastatic OC in comparison to benign ovary, revealing also a significant correlation with tumour grade and nodal involvement in S-OC patients and advanced FIGO stage in E-OC patients.

Although dysregulation of PDCD10 expression has been frequently observed in many cancer types, the role of PDCD10 in human tumors is still controversial. In fact, whereas PDCD10 has been shown to be up-regulated in oral, colorectal and pancreatic cancer [34–36], the loss of PDCD10 has been associated to the progression of glioblastoma [37]. PDCD10 has been shown to be the target for the tumor suppressor activity of miR-222-3p in ovarian cancer [7], of miR-103 in prostate or lung cancer [38,39] and of miR-26a-5p and of miR-26b-5p in bladder cancer [40]. On the other hand, mir-425-5p-induced up-regulation of PDCD10 promotes chemo-resistance in colorectal cancer cells [41].

The results presented in this study contribute to demonstrate that PDCD10 promotes cancer growth, being markedly up-regulated in both primary and metastatic OC lesions. Furthermore, we also provide evidence that PDCD10 positively regulates cell proliferation, migration and invasion of human OC cells *in vitro* and tumor growth in xenograft experiments. These conclusions are supported by experiments of manipulation of PDCD10 expression with shRNA, in which the suppression of PDCD10 reduced anchorage-dependent and -independent growth of 2 OC cell lines, markedly impaired the ability to migrate and invade through reconstituted basal membrane and decreased the growth of xenografted cells in immunodeficient mice.

As to the mechanism, our results suggest that the ERK1/2 pathway is involved in PDCD10-dependent regulation of proliferation and that the RhoA pathway is involved in PDCD10-dependent regulation of migration. PDCD10 interacts and stabilizes MST4 [42], a protein that specifically activates ERK kinases [43]. The ERK proteins are well known regulators of mitogenesis and inducers of Cyclin D1 [44]. In ovarian cancer cells, PDCD10 silencing reduces active ERK1/2, which in turn is reflected into reduction of Cyclin D1 levels and subsequent hypophosphorylation of Rb protein, suggesting that the mechanism whereby PDCD10 promotes cancer is the deregulation of ERK signaling.

Our study also revealed that PDCD10 regulates the mode of ovarian cancer cell migration. PDCD10-dependent regulation of Rho signaling may play a pivotal role in the balance between actin polymerization and myosin contractility [45,46]. By decreasing the amount of active RhoA and of phosphorylated Cofilin and by increasing phosphorylation of MLC, PDCD10 may tip the balance toward actin depolymerization and myosin contraction, thus facilitating migration. These observations were concordant with previous lines of evidence demonstrating PDCD10 role in inhibiting RhoA signaling [47,48]. In breast cancer cells, TRIM59-dependent stabilization of PDCD10 induces inhibition of RhoA signaling that results in either mesenchymal or lamellipodia movement [49]. Moreover, a recent work from Fan L. et al. demonstrated that SNAI2 enhances ovarian cancer cells migration through the axis miR-222-3/PDCD10 [7]. All together our results identifies PDCD10 as an important player in cancer development and a promising therapeutic target. In consideration of the relevant role of microRNAs in PDCD10 regulation [7, 38–40], a promising therapeutic option is represented by microRNAs such as miR-222-3p, miR103 and miR-26a/b-5p targeting PDCD10. Other therapeutic candidates are represented by ERK inhibitors, especially for their potential in overcoming resistance towards drugs targeting upstream molecules [50]. On the basis of ERK mediated effects in both proliferation and migration of cells overexpressing PDCD10, the use of ERK inhibitors might be a valuable option.

In conclusion, this study allowed the identification of novel genes subjected to CNA in OC and thus potentially relevant for the development of this cancer. In particular, the results reported here point to a prominent role for PDCD10 as a *bona fide* oncogene in OC.

Declaration of Competing Interest

The authors have no conflict of interest to disclose.

CRediT authorship contribution statement

Carmela De Marco: Investigation, Visualization, Formal analysis, Writing - original draft, Funding acquisition. **Pietro Zoppoli:** Software, Formal analysis. **Nicola Rinaldo:** Investigation. **Sandro Morganella:** Methodology, Software. **Matteo Morello:** Investigation. **Valeria Zuccalà:** Investigation. **Maria Vincenza Carriero:** Investigation. **Donatella Malanga:** Investigation. **Roberta Chirillo:** Investigation. **Paola Bruni:** Resources. **Carmine Malzoni:** Resources. **Dolores Di Vizio:** Investigation, Writing - review & editing. **Roberta Venturella:** Resources, Funding acquisition. **Fulvio Zullo:** Resources. **Antonia Rizzuto:** Resources. **Michele Ceccarelli:** Data curation, Resources. **Gennaro Ciliberto:** Writing - review & editing. **Giuseppe Viglietto:** Conceptualization, Methodology, Supervision, Funding acquisition, Writing - review & editing, Project administration.

Aknowledgements

We thank the Molecular Pathology Unit of the Molecular Medicine Program at the European Institute of Oncology for providing the Ovary2_TMA slices and Dr. Valter Agosti for his support in cell cycle analysis.

Funding

This work was supported by grants from Ministero dell'Istruzione, dell'Università e della Ricerca (MIUR) (2010W4J4RM_001 and PON01_27082) to GV and from Ministero Italiano della Salute (GR-2018-12368359) to CDM and RV.

Supplementary materials

Supplementary material associated with this article can be found, in the online version, at doi:10.1016/j.tranon.2021.101013.

References

[1] G Ciriello, ML Miller, BA Aksoy, Y Senbabaoglu, N Schultz, C Sander, Emerging landscape of oncogenic signatures across human cancers, Nat. Genet. 45 (2013) 1127–1133.
[2] R Vang, M Shih Ie, RJ Kurman, Ovarian low-grade and high-grade serous carcinoma: pathogenesis, clinicopathologic and molecular biologic features, and diagnostic problems, Adv. Anat. Pathol. 16 (2009) 267–282.
[3] KL Gorringe, S Jacobs, ER Thompson, A Sridhar, W Qiu, DY Choong, IG Campbell, High-resolution single nucleotide polymorphism array analysis of epithelial ovarian cancer reveals numerous microdeletions and amplifications, Clin. Cancer Res. 13 (2007) 4731–4739.
[4] Integrated genomic analyses of ovarian carcinoma, Nature 474 (2011) 609–615.
[5] F Bergametti, C Denier, P Labauge, M Arnoult, S Boetto, M Clanet, P Coubes, B Echenne, R Ibrahim, B Irthum, et al., Mutations within the programmed cell death 10 gene cause cerebral cavernous malformations, Am. J. Hum. Genet. 76 (2005) 42–51.
[6] M Fidalgo, M Fraile, A Pires, T Force, C Pombo, J Zalvide, CCM3/PDCD10 stabilizes GCKIII proteins to promote Golgi assembly and cell orientation, J. Cell Sci. 123 (2010) 1274–1284.
[7] L Fan, H Lei, S Zhang, Y Peng, C Fu, G Shu, G Yin, Non-canonical signaling pathway of SNAI2 induces EMT in ovarian cancer cells by suppressing miR-222-3p transcription and upregulating PDCD10, Theranostics 10 (2020) 5895–5913.
[8] VW Chen, B Ruiz, JL Killeen, TR Cote, XC Wu, CN Correa, Pathology and classification of ovarian tumors, Cancer 97 (2003) 2631–2642.
[9] S Morganella, SM Pagnotta, M Ceccarelli, Finding recurrent copy number alterations preserving within-sample homogeneity, Bioinformatics 27 (2011) 2949–2956.
[10] MS Cline, B Craft, T Swatloski, M Goldman, S Ma, D Haussler, J Zhu, Exploring TCGA pan-cancer data at the UCSC cancer genomics browser, Sci. Rep. 3 (2013) 2652.
[11] C Mignogna, N Staropoli, C Botta, C De Marco, A Rizzuto, M Morelli, A Di Cello, R Franco, C Camastra, I Presta, et al., Aurora Kinase A expression predicts platinum-resistance and adverse outcome in high-grade serous ovarian carcinoma patients, J. Ovarian Res. 9 (2016) 31.

[12] CC Yao, LF Kok, MY Lee, PH Wang, TS Wu, YS Tyan, YW Cheng, MF Kung, CP Han, Ancillary p16(INK4a) adds no meaningful value to the performance of ER/PR/Vim/CEA panel in distinguishing between primary endocervical and endometrial adenocarcinomas in a tissue microarray study, Arch. Gynecol. Obstet. 280 (2009) 405–413.
[13] F Biamonte, AM Battaglia, F Zolea, DM Oliveira, I Aversa, G Santamaria, ED Giovannone, G Rocco, G Viglietto, F Costanzo, Ferritin heavy subunit enhances apoptosis of non-small cell lung cancer cells through modulation of miR-125b/p53 axis, Cell Death. Dis. 9 (2018) 1174.
[14] M Di Sanzo, I Aversa, G Santamaria, M Gagliardi, M Panebianco, F Biamonte, F Zolea, MC Faniello, G Cuda, F Costanzo, FTH1P3, a novel H-Ferritin pseudogene transcriptionally active, is ubiquitously expressed and regulated during cell differentiation, PLoS One 11 (2016) e0151359.
[15] F Biamonte, G Santamaria, A Sacco, FM Perrone, A Di Cello, AM Battaglia, A Salatino, A Di Vito, I Aversa, R Venturella, et al., MicroRNA let-7g acts as tumor suppressor and predictive biomarker for chemoresistance in human epithelial ovarian cancer, Sci. Rep. 9 (2019) 5668.
[16] CH Mermel, SE Schumacher, B Hill, ML Meyerson, R Beroukhim, G Getz, GISTIC2.0 facilitates sensitive and confident localization of the targets of focal somatic copy--number alteration in human cancers, Genome Biol. 12 (2011) R41.
[17] DA Engler, S Gupta, WB Growdon, RI Drapkin, M Nitta, PA Sergent, SF Allred, J Gross, MT Deavers, WL Kuo, et al., Genome wide DNA copy number analysis of serous type ovarian carcinomas identifies genetic markers predictive of clinical outcome, PLoS One 7 (2012) e30996.
[18] PM Haverty, LS Hon, JS Kaminker, J Chant, Z Zhang, High-resolution analysis of copy number alterations and associated expression changes in ovarian tumors, BMC Med. Genet. 2 (2009) 21.
[19] J Haley, S Tomar, N Pulliam, S Xiong, SM Perkins, AR Karpf, S Mitra, KP Nephew, AK Mitra, Functional characterization of a panel of high-grade serous ovarian cancer cell lines as representative experimental models of the disease, Oncotarget 7 (2016) 32810–32820.
[20] E Papp, D Hallberg, GE Konecny, DC Bruhm, V Adleff, M Noë, I Kagiampakis, D Palsgrove, D Conklin, Y Kinose, et al., Integrated genomic, epigenomic, and expression analyses of ovarian cancer cell lines, Cell Rep. 25 (2018) 2617–2633.
[21] S Etienne-Manneville, A Hall, Rho GTPases in cell biology, Nature 420 (2002) 629–635.
[22] V Mancikova, R Cruz, L Inglada-Perez, C Fernandez-Rozadilla, I Landa, J Cameselle-Teijeiro, C Celeiro, S Pastor, A Velazquez, R Marcos, et al., Thyroid cancer GWAS identifies 10q26.12 and 6q14.1 as novel susceptibility loci and reveals genetic heterogeneity among populations, Int. J. Cancer 137 (2015) 1870–1878.
[23] J Vijayakrishnan, R Kumar, MY Henrion, AV Moorman, PS Rachakonda, I Hosen, MI da Silva Filho, A Holroyd, SE Dobbins, R Koehler, et al., A genome-wide association study identifies risk loci for childhood acute lymphoblastic leukemia at 10q26.13 and 12q23.1, Leukemia 31 (2017) 573–579.
[24] L Chen, C Li, R Zhang, X Gao, X Qu, M Zhao, C Qiao, J Xu, J Li, miR-17-92 cluster microRNAs confers tumorigenicity in multiple myeloma, Cancer Lett. 309 (2011) 62–70.
[25] E Rao, C Jiang, M Ji, X Huang, J Iqbal, G Lenz, G Wright, LM Staudt, Y Zhao, TW McKeithan, et al., The miRNA-17 approximately 92 cluster mediates chemoresistance and enhances tumor growth in mantle cell lymphoma via PI3K/AKT pathway activation, Leukemia 26 (2012) 1064–1072.
[26] T Sareeboot, P Punyarit, S Petmitr, DNA amplification on chromosome 13q31.1 correlated with poor prognosis in colorectal cancer, Clin. Exp. Med. 11 (2011) 97–103.
[27] A Miloloza, M Rosner, M Nellist, D Halley, G Bernaschek, M Hengstschlager, The TSC1 gene product, hamartin, negatively regulates cell proliferation, Hum. Mol. Genet. 9 (2000) 1721–1727.
[28] EB Kuznetsova, TV Kekeeva, SS Larin, VV Zemliakova, OV Babenko, MV Nemtsova, DV Zaletaev, VV Strel'nikov, [Novel methylation and expression markers associated with breast cancer], Mol. Biol. (Mosk) 41 (2007) 624–633.
[29] N Amira, G Cancel-Tassin, S Bernardini, B Cochand-Priollet, H Bittard, P Mangin, G Fournier, A Latil, O Cussenot, Expression in bladder transitional cell carcinoma by real-time quantitative reverse transcription polymerase chain reaction array of 65 genes at the tumor suppressor locus 9q34.1-2: identification of 5 candidates tumor suppressor genes, Int. J. Cancer 111 (2004) 539–542.
[30] MJ Kim, HS Yoon, G Lim, SY Kim, HJ Lee, JT Suh, J Lee, WI Lee, TS Park, ABL1 gene deletion without BCR/ABL1 rearrangement in a young adolescent with precursor B-cell acute lymphoblastic leukemia: clinical study and literature review, Cancer Genet. Cytogenet. 196 (2010) 184–188.
[31] PS Felicio, LT Bidinotto, ME Melendez, RS Grasel, N Campacci, HCR Galvao, C Scapulatempo-Neto, RM Dufloth, AF Evangelista, EI Palmero, Genetic alterations detected by comparative genomic hybridization in BRCAX breast and ovarian cancers of Brazilian population, Oncotarget 9 (2018) 27525–27534.
[32] W Chen, J Ding, L Jiang, Z Liu, X Zhou, D Shi, DNA copy number profiling in microsatellite-stable and microsatellite-unstable hereditary non-polyposis colorectal cancers by targeted CNV array, Funct. Integr. Genomics 17 (2017) 85–96.
[33] F Zazzeroni, D Nicosia, A Tessitore, R Gallo, D Verzella, M Fischietti, D Vecchiotti, L Ventura, D Capece, A Gulino, et al., KCTD11 tumor suppressor gene expression is reduced in prostate adenocarcinoma, Biomed. Res. Int. 2014 (2014) 380398.
[34] AJ Aguirre, C Brennan, G Bailey, R Sinha, B Feng, C Leo, Y Zhang, J Zhang, JD Gans, N Bardeesy, et al., High-resolution characterization of the pancreatic adenocarcinoma genome, PNAS 101 (2004) 9067–9072.
[35] J Cardoso, J Boer, H Morreau, R Fodde, Expression and genomic profiling of colorectal cancer, Biochim. Biophys. Acta 1775 (2007) 103–137.
[36] S Gibson, EJ Shillitoe, Analysis of apoptosis-associated genes and pathways in oral cancer cells, J. Oral Pathol. Med. 35 (2006) 146–154.
[37] N Lambertz, N El Hindy, I Kreitschmann-Andermahr, KP Stein, P Dammann, N Oezkan, O Mueller, U Sure, Y Zhu, Downregulation of programmed cell death 10 is associated with tumor cell proliferation, hyperangiogenesis and peritumoral edema in human glioblastoma, BMC Cancer 15 (2015) 759.
[38] X Fu, W Zhang, Y Su, L Lu, D Wang, H Wang, MicroRNA-103 suppresses tumor cell proliferation by targeting PDCD10 in prostate cancer, Prostate 76 (2016) 543–551.
[39] D Yang, JJ Wang, JS Li, QY Xu, miR-103 Functions as a tumor suppressor by directly targeting programmed cell death 10 in NSCLC, Oncol. Res. 26 (2018) 519–528.
[40] K Wu, XY Mu, JT Jiang, MY Tan, RJ Wang, WJ Zhou, X Wang, YY He, MQ Li, ZH Liu, miRNA26a5p and miR26b5p inhibit the proliferation of bladder cancer cells by regulating PDCD10, Oncol. Rep. 40 (2018) 3523–3532.
[41] Y Zhang, X Hu, X Miao, K Zhu, S Cui, Q Meng, J Sun, T Wang, MicroRNA-425-5p regulates chemoresistance in colorectal cancer cells via regulation of programmed cell death 10, J. Cell. Mol. Med. 20 (2016) 360–369.
[42] X Ma, H Zhao, J Shan, F Long, Y Chen, Y Chen, Y Zhang, X Han, D Ma, PDCD10 interacts with Ste20-related kinase MST4 to promote cell growth and transformation via modulation of the ERK pathway, Mol. Biol. Cell 18 (2007) 1965–1978.
[43] JL Lin, HC Chen, HI Fang, D Robinson, HJ Kung, HM Shih, MST4, a new Ste20-related kinase that mediates cell growth and transformation via modulating ERK pathway, Oncogene 20 (2001) 6559–6569.
[44] JC Chambard, R Lefloch, J Pouysségur, P Lenormand, ERK implication in cell cycle regulation, Biochim. Biophys. Acta 1773 (2007) 1299–1310.
[45] AJ Ridley, Rho GTPase signalling in cell migration, Curr. Opin. Cell Biol. 36 (2015) 103–112.
[46] K O'Connor, M Chen, Dynamic functions of RhoA in tumor cell migration and invasion, Small GTPases 4 (2013) 141–147.
[47] RA Stockton, R Shenkar, IA Awad, MH Ginsberg, Cerebral cavernous malformations proteins inhibit Rho kinase to stabilize vascular integrity, J. Exp. Med. 207 (2010) 881–896.
[48] R Shenkar, C Shi, T Rebeiz, RA Stockton, DA McDonald, AG Mikati, L Zhang, C Austin, AL Akers, CJ Gallione, et al., Exceptional aggressiveness of cerebral cavernous malformation disease associated with PDCD10 mutations, Genet. Med. 17 (2015) 188–196.
[49] P Tan, Y Ye, L He, J Xie, J Jing, G Ma, H Pan, L Han, W Han, Y Zhou, TRIM59 promotes breast cancer motility by suppressing p62-selective autophagic degradation of PDCD10, PLoS Biol. 16 (2018) e3000051.
[50] F Liu, X Yang, M Geng, M Huang, Targeting ERK, an Achilles' Heel of the MAPK pathway, in cancer therapy, Acta pharmaceutica Sinica B 8 (2018) 552–562.